10.31195/ejejfs.603510

Eurasian Journal of Forest Science

2019 7(2): 187-204

http://dergipark.gov.tr/ejejfs

# Using of high-resolution satellite images in object-based image analysis

Huseyin Yurtseven[1*], Hakan Yener[1]

[1*)]*Department of Surveying and Cadastre, Faculty of Forestry, Istanbul University - Cerrahpasa, 34473 Istanbul, Turkey*
*Corresponding author:* huseyiny@istanbul.edu.tr

**Abstract**
Remote Sensing technologies have been used quite a long time in forestry applications. While the more acquired data can be obtained with traditional survey and photogrammetric techniques, they required relatively more manpower and time consuming.
The most important characteristics of this research will bring the new opportunities for forestry applications by using the object-based classification methods with multispectral satellite images that have high spatial resolution (<1meter). In this individual tree and forest stand based research, the solutions searched with using very high-resolution (VHR) satellite images for time-consuming problems in forestry applications.
**Keywords:** Worldview-2, Object-based image analysis, Tree crown

## INTRODUCTION

Remote sensing provides a useful source of data from which updated land-cover information can be extracted for assessing and monitoring vegetation changes. In the past several decades, aerial photo interpretation has played an important role in detailed vegetation mapping (Sandmann and Lertzman, 2003). Nowadays, with the development of technological possibilities, geometric, radiometric, temporal and spectral resolutions in satellite and sensor systems have increased. With these developments, satellite remote sensing data can provide more and variety of information than analog aerial photographs (Yurtseven, 2014).

In remote sensing studies, object-based classification approaches are used in addition to pixel-based classification approaches. The main reason for using object-based approaches is that image objects are characterized by a number of additional features, such as texture and form, beyond the pure spectral information. All this additional information can hardly be exploited using pixel-based approaches (Baatz and Schäpe, 1999; Wong *et al.*, 2003). In object-based image analysis (OBIA), unlike traditional image processing techniques, the smallest processing unit is image objects or segments rather than pixels (Baatz *et al.*, 2004). Unlike pixel-based methods, the image is analyzed in homogeneous segments (objects) by shape, texture and contextual models. This provides a sophisticated base for image analysis (Yan *et al.*, 2006).

OBIA of multispectral (MS) imagery has entered the remote sensing literature at a very early stage (Kettig and Landgrebe, 1976; Haralick, 1983; Haralick and Shapiro, 1985; Levine and Nazif, 1985; Strahler *et al.*, 1986; McKeown Jr *et al.*, 1989; Pal and Pal, 1993; Câmara *et al.*, 1996; Hay *et al.*, 1996; Lobo *et al.*, 1996; Ryherd and Woodcock, 1996; Wulder, 1998; Aplin *et al.*, 1999; Baltsavias, 2004). Multispectral imagery supports not only enhanced display of scene content, but also quantitative analysis

based on the intrinsic spectral characteristics of imaged objects (Schott, 2007). In this context, due to the simpler implementation of conventional pixel-based approaches and require less computational power, object-based approaches have not been given due attention (Lobo, 1997). Traditional pixel-oriented algorithms and analytic techniques cannot take full advantage of the increased spatial coherence of very high-resolution imagery (Nussbaum, 2008).

In the literature, it is seen that object-based approaches are generally used to obtain stand-based data in forest areas (Chubey *et al.*, 2006; Wulder *et al.*, 2008; Immitzer *et al.*, 2016; Gudex-Cross *et al.*, 2017). However, the main potential of OBIA is emerged by the use of very high-resolution (VHR) (spectral, radiometric and spatial) imagery (Blaschke *et al.*, 2014). The number of remote sensing systems with very high spatial resolution has increased, as a result of advances in sensor technologies. Therefore, individual tree-based studies can also be performed by using VHR satellite imagery (Ke and Quackenbush, 2007; Li *et al.*, 2015). The acquisition of individual tree crown parameters using VHR data with OBIA techniques is an ongoing research topic. In this context, many techniques have been developed, such as template matching (Pollock, 1996), multiple-scale analysis (Brandtberg and Walter, 1998), valley following (Gougeon, 1995), spatial clustering (Culvenor, 2002), region growing (Erikson, 2003), marked point processes (Perrin *et al.*, 2006), Markov random fields (Descombes and Pechersky, 2006), radial brightness distribution (Pinz, 1989), contour tree (Wu *et al.*, 2016). Most of the proposed algorithms are used combinations of these techniques.

The accuracy of detailed vegetation classification with very high-resolution imagery is highly dependent on the segmentation quality, sample size, sampling method, classification framework, and ground vegetation distribution and mixture (Yu *et al.*, 2006; Rafieyan *et al.*, 2009a; Rafieyan *et al.*, 2009b).

In this study, it is aimed to determine the usage potential of the above-mentioned combination (VHR satellite imagery and OBIA) in forest areas. In this context, WorldView-2 (WV-2) MS imagery were employed. OBIA-based classifications were made on this imagery to generate stand and individual tree based information. Accuracy analyzes were performed to evaluate the problems and dilemmas and all the results were discussed.

## Study area and data

The study area is located in north of Istanbul in Turkey and covered western part of the forested area called the Belgrade Forests (Figure 1). Elevations, ranges from the sea level up to 237.17 m. Main species that show stand formation in the study area are: Oak species (*Quercus* sp.), Oriental beech (*Fagus orientalis*), Common hornbeam (*Carpinus betulus*), Anatolian chestnut (*Castanea sativa*), Black pine (*Pinus nigra*), Stone pine (*Pinus pinea*), Turkish pine (*Pinus brutia Ten.*), Maritime pine (*Pinus pinaster*), False acacia (*Robinia pseudoacacia*), Linden species (*Tilia* sp.), Strawberry tree (*Arbutus unedo*) and Oriental spruce (*Picea orientalis*).

In this study, stereoscopically acquired a pair of WV-2 satellite data were used. Data acquisitions were performed on June 6, 2011 at 10:59 (A.M.) (with 10.0 off nadir angle) and 11:00 (A.M.) (with 21.1 off nadir angle) local time. WV-2 imagery have 8 MS and a panchromatic sensor bands (see Table 1 for more details). Further details about the sensor can be found on Updike and Comp (2010).

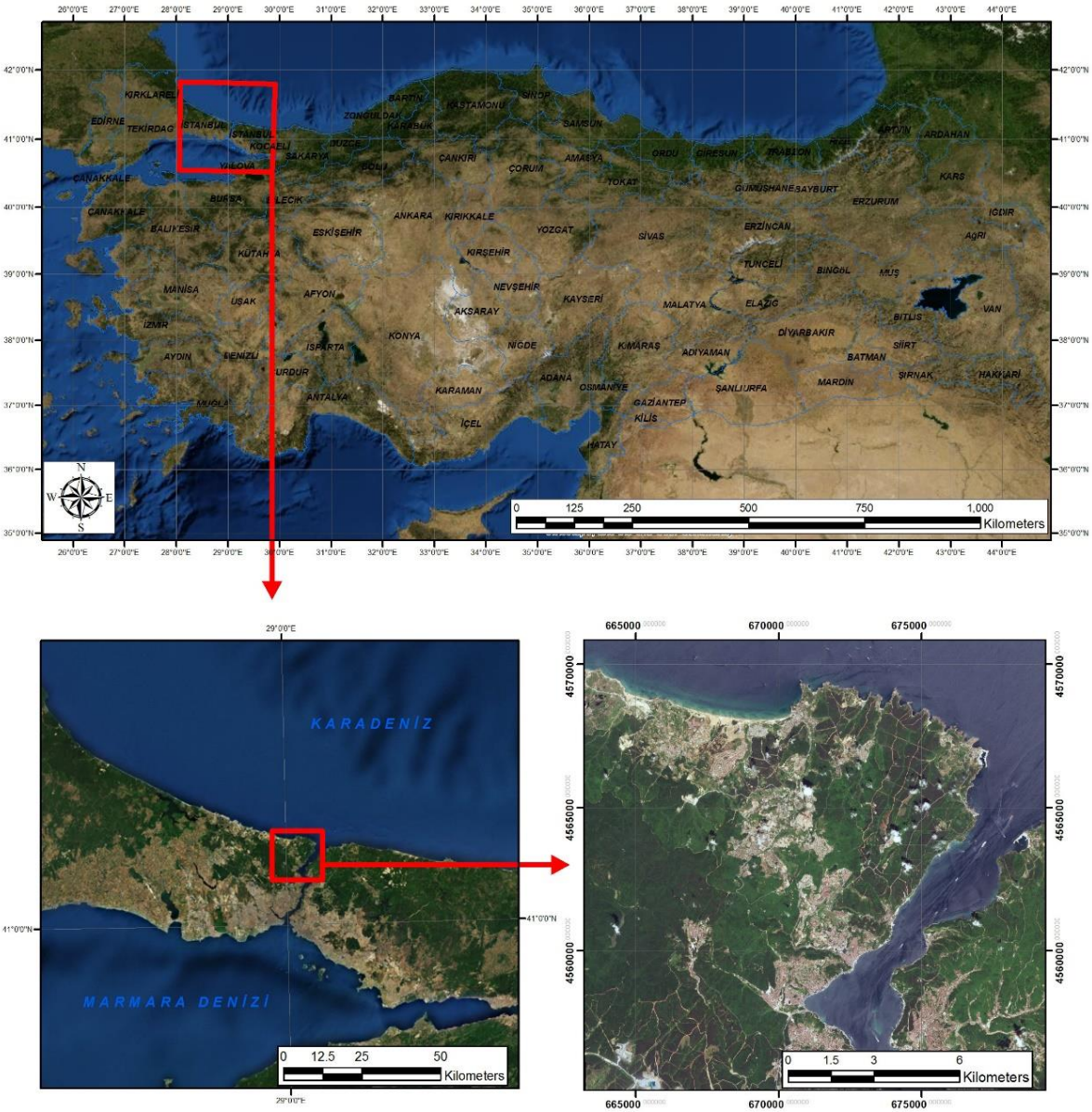


Figure 1. Study area.

Table 1. Characteristics of WorldView-2 imagery.

| Spectral Bands | Wavelength (nm) | Spatial Resolution at Nadir Look (m) |
|---|---|---|
| Coastal | 400 - 450 | 1.84 |
| Blue | 450 - 510 | 1.84 |
| Green | 510 - 580 | 1.84 |
| Yellow | 585 - 625 | 1.84 |
| Red | 630 - 690 | 1.84 |
| Red Edge | 705 - 745 | 1.84 |
| Near-IR1 | 770 - 895 | 1.84 |
| Near-IR2 | 860 - 1040 | 1.84 |
| Panchromatic | 450 - 800 | 0.46 |

## Methodology

Within the scope of the study, our approach consists of the following main steps (Figure 2): DSM generation with photogrammetric processing, atmospheric and topographic correction, pan-sharpening, generation of image indices, OBIA and classifications.

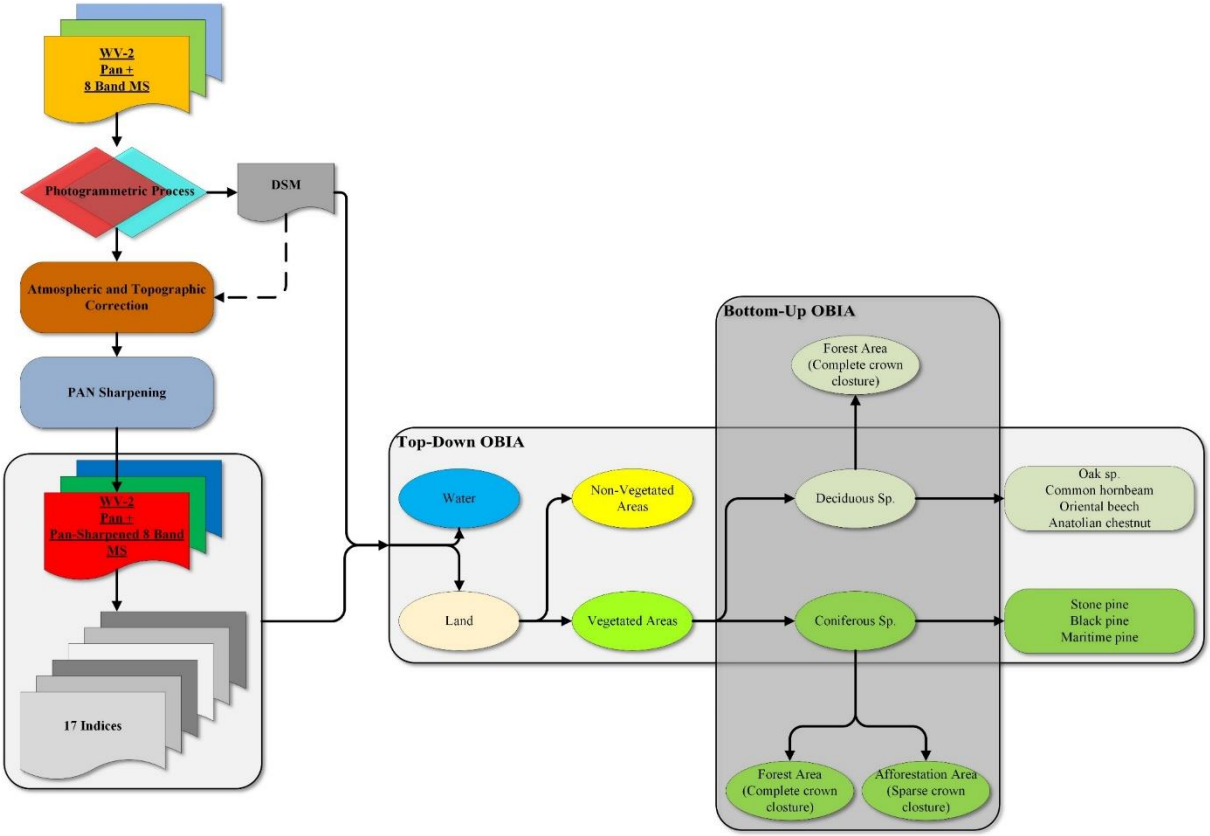


Figure 2. Main workflow steps.

As is known, the basic radiation source of passive remote sensing systems is the sun (Erdin, 1986). Radiation reflected or radiated from the earth reaches the sensors in a manner attenuated by absorption or scattering by atmospheric components (humidity, pressure, temperature, molecular differences) (Bakker *et al.*, 2009). In addition, topographic differences and location on the earth also affect reflection. Elimination of these effects allows accurate evaluation of remote sensing data (Campbell and Wynne, 2012). Especially in VHR satellite imagery, atmospheric and topographic factors adversely affect radiometry (Neubert and Meinel, 2005). Although many different approaches are used in the removal of atmospheric and topographic effects from images, in this study, ATCOR3 model, which provides fast and accurate results, was used to eliminate atmospheric and topographic errors in satellite imagery. Detailed modeling and explanations of the method are described by Richter and Schläpfer (2014). At the stage of atmospheric and topographic corrections, a digital surface model (DSM) is needed. By using state of art technologies such as LIDAR (Light Detection and Ranging) and SAR (Synthetic Aperture Radar), it is possible to generate digital surface and terrain models very precisely. However, in some cases such data may not be accessible for a specific area. Therefore, in this study, DSM has been generated by using stereoscopically acquired panchromatic WV-2 data. In this context, ERDAS Imagine Photogrammetry and Stereo Analyst for ERDAS Imagine software packages were employed to generate DSM.

Spatial resolution is a key feature to obtain detailed information about spatial objects. In this context, spatial resolution should be maximized in order to obtain detailed and precise information. When working with multi-resolution data, resolution merging techniques are used to increase spatial detail. The main interest of merging multi-resolution image data is to generate composite images of improved interpretability (Welch and Ehlers, 1987; Kaczynski *et al.*, 1995; de Béthune *et al.*, 1998). In addition, it is desirable to maintain the spectral quality of the images with the highest possible spatial detail (Cliche *et al.*, 1985). Garguet-Duport *et al.* (1996) indicated that preservation of spectral information and properties is particularly important for vegetation analysis. In this context, the Hyperspherical Color Space (HCS) technique, which was developed specifically for WV-2 satellite data and described by Padwick *et al.* (2010) and Deskevich and Padwick (2012), was used in pan-sharpening process.

Vegetation absorb electromagnetic energy, especially in the part of the spectrum between 450-670 nm wavelengths. This cut is called chlorophyll absorption band. Between 700-1300 nm wavelengths, they reflect about half of the incoming energy. In order to enhance this spectral difference in multi-band employed remote sensing studies, image indices are generated and used in analysis (Sader and Winne, 1992; Koç, 1997; Hayes *et al.*, 2002). When the multispectral data of the WorldView-2 satellite is examined, it is seen that it has suitable spectral characteristics for a total of close to 300 indices including single bands (Henrich *et al.*, 2015). In deciding on the image indices used in the classification, the most commonly used indices in the literature were evaluated for their suitability for the study (Rouse Jr *et al.*, 1974; Tucker, 1979; Jackson *et al.*, 1983; Sellers, 1985; Kaufman and Tanré, 1996; Huete *et al.*, 1997; Wolf, 2010; Jones *et al.*, 2011; Zhou *et al.*, 2012). In this context, 17 image indexes were selected and used in this study (Table 2). After the generation of an input datasets OBIA were performed with the eCognition software. OBIA can be examined in two stages: segmentation and classification. The purpose of the segmentation process is to generate meaningful objects from the image pixels. There are two basic segmentation principles, which are top-down and bottom-up strategies (Trimble, 2012). In the top-down approach, which has been developed on the strategy of dividing objects from smaller pieces into large pieces, the image can be considered as a single large object or it can be applied in previously generated image objects. The bottom-up strategy, in which small objects are combined to form larger objects, is used to generate larger and homogeneous objects than image pixels or previously generated image objects. Classification can be used to generate more meaningful image objects by assisting segmentation, or it can be used for direct classification of generated image objects. In the OBIA processes, various features related to image objects can be used, such as spectral, geometric, positional, textural, and thematic features. Nevertheless, there is no accepted approach in the literature as to which features should be used for classification (Blaschke, 2010).

## Results and Discussion

According to the main workflow of this study the first step is photogrammetric analysis and DSM generation. Photogrammetric operations were performed by using rational polynomial coefficients (RPC) parameters, which were supplied with imagery, and 23 ground control points (GCP). GCP coordinates were collected by using NRTK (Network Real Time Kinematic) Global Navigation Satellite System (GNSS) receiver according to the TUREF (Turkish National Reference Frame) TM30 (EPSG: 5254) coordinate system and Turkey CORS (Continuously Operating Reference Stations) network system. In this context, coordinate transformations to WGS 84 geographic coordinates were performed in ArcGIS software. According to the photogrammetric process results aerial triangulation were accomplished with 0.06 m Root Mean Square Error (RMSE) and total RMSE of GCPs were 0.61 m in horizontal plane and 0.52 m in vertical. As a result of photogrammetric operations, 5 m resolution DSM was generated to be used in atmospheric and topographic corrections and OBIA analysis.

Table 2. Description of all indices.

| Index Name | Formula |
|---|---|
| Difference Vegetation Index (DVI) | $DVI = (NIR1 - Red)$ |
| Normalized Difference Vegetation Index (NDVI) | $NDVI = \frac{(NIR1 - Red)}{(NIR1 + Red)}$ |
| WorldView Improved Normalized Difference Vegetation Index (WVINDVI) | $WVINDVI = \frac{(NIR2 - Red)}{(NIR2 + Red)}$ |
| Renormalized Difference Vegetation Index (RDVI) | $RDVI = \frac{(NIR1 - Red)}{\sqrt{(NIR1 + Red)}}$ |
| Transformed Normalized Difference Vegetation Index (TNDVI) | $TNDVI = \sqrt{\frac{(NIR1 - Red)}{(NIR1 + Red) + 0{,}5}}$ |
| Ratio Vegetation Index (RVI) | $RVI = \frac{Red}{NIR1}$ |
| Iron Oxide (IO) | $IO = \frac{Red}{Blue}$ |
| Soil Adjusted Vegetation Index (SAVI) | $SAVI = \frac{(NIR1 - Red)}{(NIR1 + Red + L)} * (1 + L) \quad L = 0{,}5$ |
| Modified Soil Adjusted Vegetation Index (MSAVI2) | $MSAVI2 = \frac{(2 * NIR1 + 1 - \sqrt{(2 * NIR1 + 1)^2 - 8 * (NIR1 - Red)})}{2}$ |
| Normalized Difference Soil Index (NDSI) – WorldView Soil Index (WVSI) | $NDSI = WVSI = \frac{(Yellow - Green)}{(Yellow + Green)}$ |
| R31 | $R31 = \frac{Red\ Edge}{Yellow}$ |
| Simple Ratio Index (SRI) | $SRI = \frac{NIR1}{Red}$ |
| Square Root of Simple Ratio Index (SQRT(SRI)) | $SQRT(SRI) = \sqrt{\frac{NIR1}{Red}}$ |
| Normalized Difference Water Index (NDWI) – WorldView Water Index (WVWI) | $NDWI = WVWI = \frac{(NIR2 - Coastal)}{(NIR2 + Coastal)}$ |
| Non-Homogeneous Feature Difference (NHFD) | $NHFD = \frac{(Red\ Edge - Coastal)}{(Red\ Edge + Coastal)}$ |
| Atmospherically Resistant Vegetation Index (ARVI) | $ARVI = \frac{NIR2 - (2Red - Blue)}{NIR2 + (2Red - Blue)}$ |
| Anthocyanin Reflectance Index (ARI) | $ARI = \left(\frac{1}{Green}\right) - \left(\frac{1}{Red}\right)$ |

Two different WV-2 images covering the same area dated June 6, 2011 were used in the study. The cloud formations in the northern and northeastern regions are especially noteworthy. Although the cloudiness ratios in each image were below 10%, the fact that the cloud formations are fragmented constitutes the biggest negativity in the images. As a result of examinations on the images, approximately 500 hectares of areas were identified which should be masked within the boundaries of the selected study area (areas under the cloud and areas under the cloud shadow). These areas were covered approximately 3% of the study area and were masked out in the imagery at the analysis stage (Figure 3).

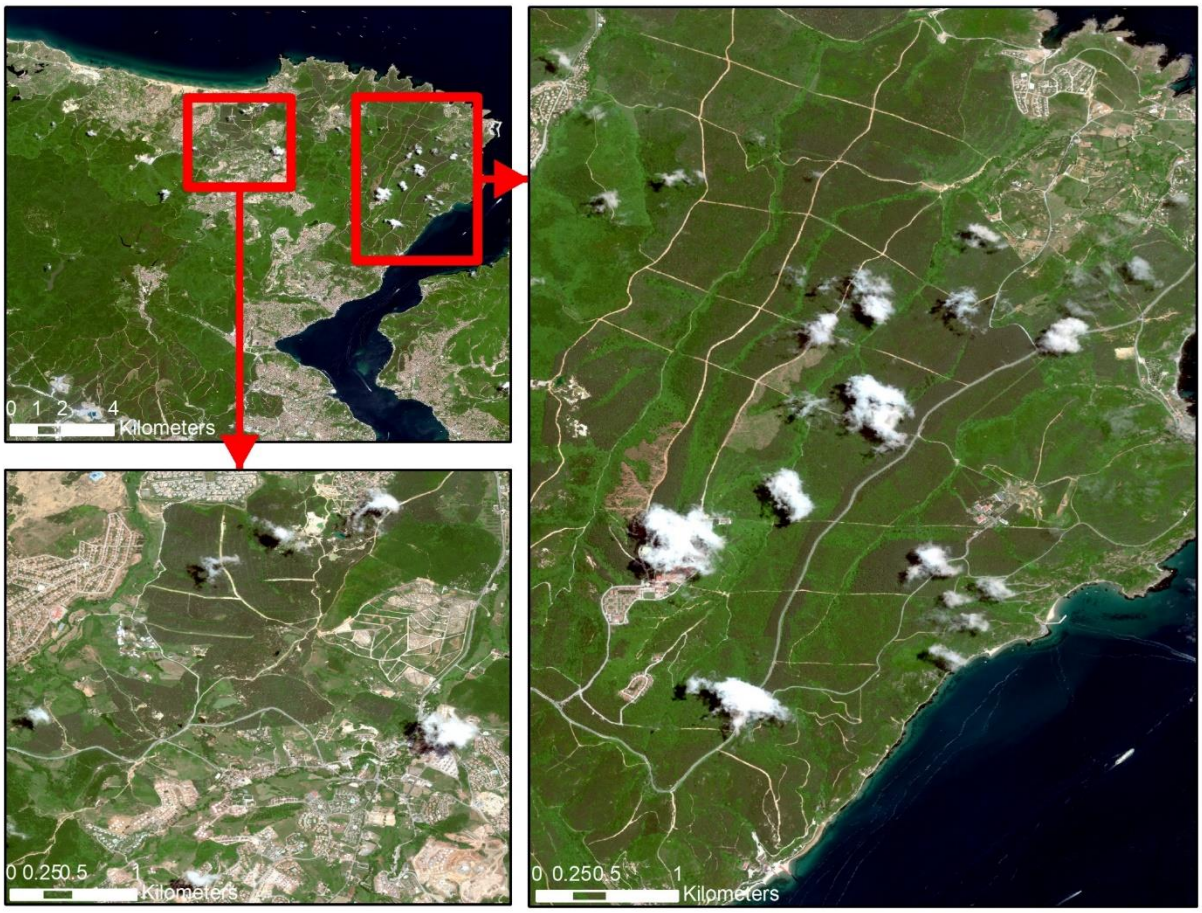


Figure 3. Cloud formations.

Cloud formations were also caused problematic formations on the photogrammetric DSM. In this context, defective areas were corrected by using DEM data, which were generated by the Greater Municipality of Istanbul (Figure 4).

The generated DSM and DSM derived slope, aspect, skyview and shadow data were employed in ATCOR3 and atmospheric and topographic correction operations were performed. The other ATCOR3 input parameters are presented in Table 3. According to ATCOR3 results, 73.2 % of image land pixels were clear land, 26.8 % image land pixels were hazy land and 32 % of image area excluded which are clouds and water bodies.

After the completion of atmospheric and topographic correction processes, pan-sharpening process was performed. At this stage, HCS resolution merge and some image enhancement techniques were combined, to achieve the highest possible spatial resolution and the highest possible spectral separability. As a result of the intensive studies carried out at this stage, application of the following methodological combination were accepted in resolution merge process (Figure 5).

As mentioned by Lillesand *et al.* (2014) the goal of image enhancement is to improve the visual interpretability of an image by increasing the apparent distinction between the features in the scene. With the methodological combination applied in this context, the spatial resolution of multispectral data increased from 2 m to 0.25 m, while the interpretability of the imagery was increased (Figure 6). In addition, the file size of the pan-sharpened multispectral data increased to 120 GB. Therefore, a high processing power is required during the processing of the imagery.

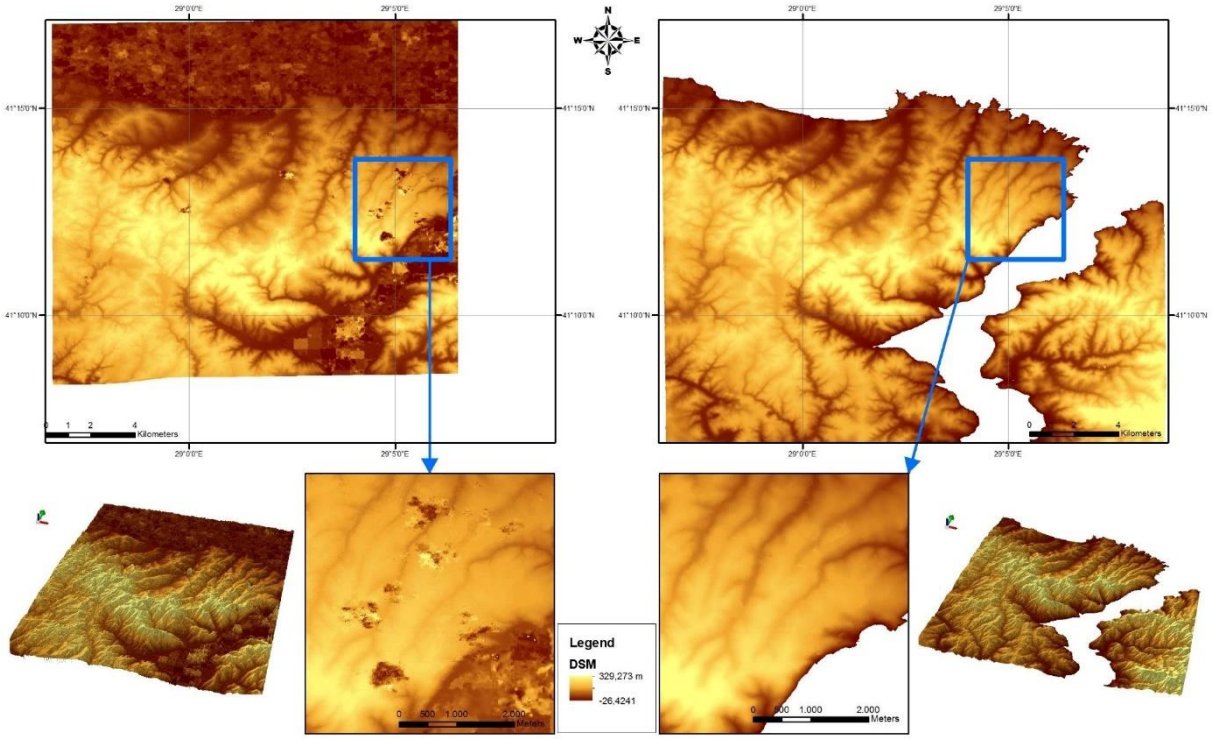


Figure 4. Photogrammetric uncorrected DSM (Left), Corrected DSM (Right).

Table 3. ATCOR3 parameters.

| Parameter | Value |
|---|---|
| Sensor | WorldView-2 MS |
| Solar Zenith Angle | 20,8 ˚ |
| Solar Azimuth Angle | 148,7 ˚ |
| Sensor Tilt Angle | 21,1 ˚ |
| Satellite Azimuth Angle | 175,3 ˚ |
| Scene Visibility | 59 |
| Model for Solar Region | Urban / Midlat Summer Urban |
| Haze Removal | Yes |
| Cloud Threshold | 16 |
| Water Threshold | 4 |

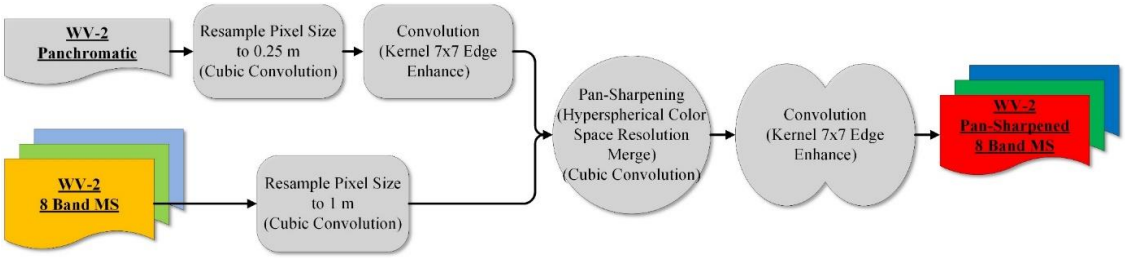


Figure 5. Pan-sharpening and image enhancement processes.

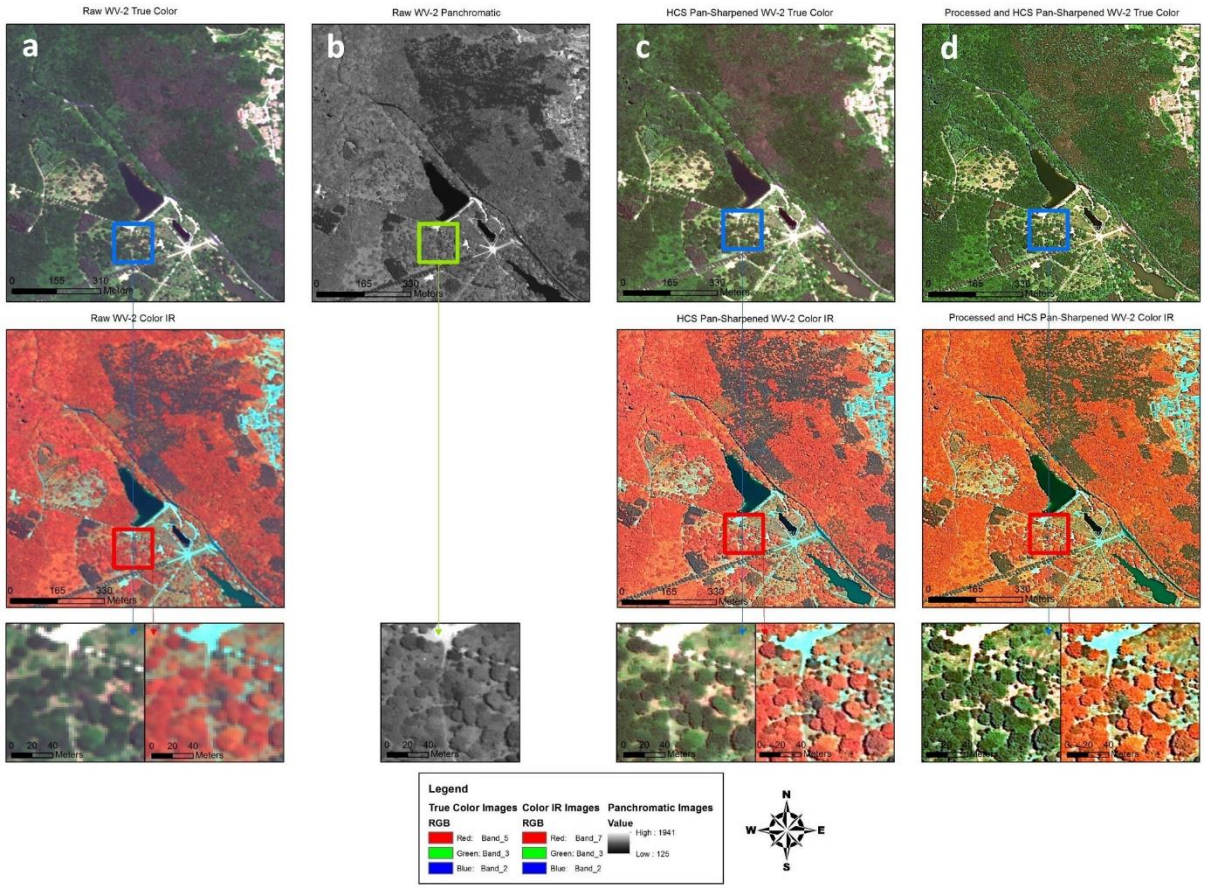


Figure 6. Detail comparisons of raw MS (a), panchromatic (b), standard HCS (c) and the enhancement combined HCS (d) imagery.

After the preparation of the images for the analysis process, we proceeded to the OBIA stage. Since there is no standard method followed in the OBIA operation, according to the data and the desired outputs at the end of the study, the algorithm combinations and workflow are created according to the knowledge and ability of the operator (Navulur, 2007; Blaschke *et al.*, 2008). At this stage, it was decided to use two different approaches in the study, which are top-down and bottom-up strategies. With the top-down approach, it was aimed to obtain stand or species -based information by a hierarchical classification strategy. Differently, with the bottom-up approach, it was aimed to obtain information on individual tree basis in specifically selected areas. However, in the selection of specific areas the data obtained with the top-down approach were used to serve the bottom-up approach (Figure 2).

Before the OBIA, 17 image indexes were generated to support the classification (Appendix 1-Image Indices). The selection of the bands and coefficients to be used in segmentation and classification stages requires a very intensive study. The parameters to be used in these stages were decided by test-observe-interpret combination. In this context, the best combination of band and parameter was determined for each class and classifications were made.

In accordance with the hierarchical model, firstly, land, water and vegetation areas were classified. Imagery were segmented by multiresolution and spectral difference segmentation to generate image objects to be used in the classification. A total of 141 training object were selected in three different classes within the study area. 47 of these are for Land, 84 for Vegetation and 10 for Water class. In this context classifications were accomplished with 99.27% overall classification accuracy and 0.9889 Kappa (Figure 7).

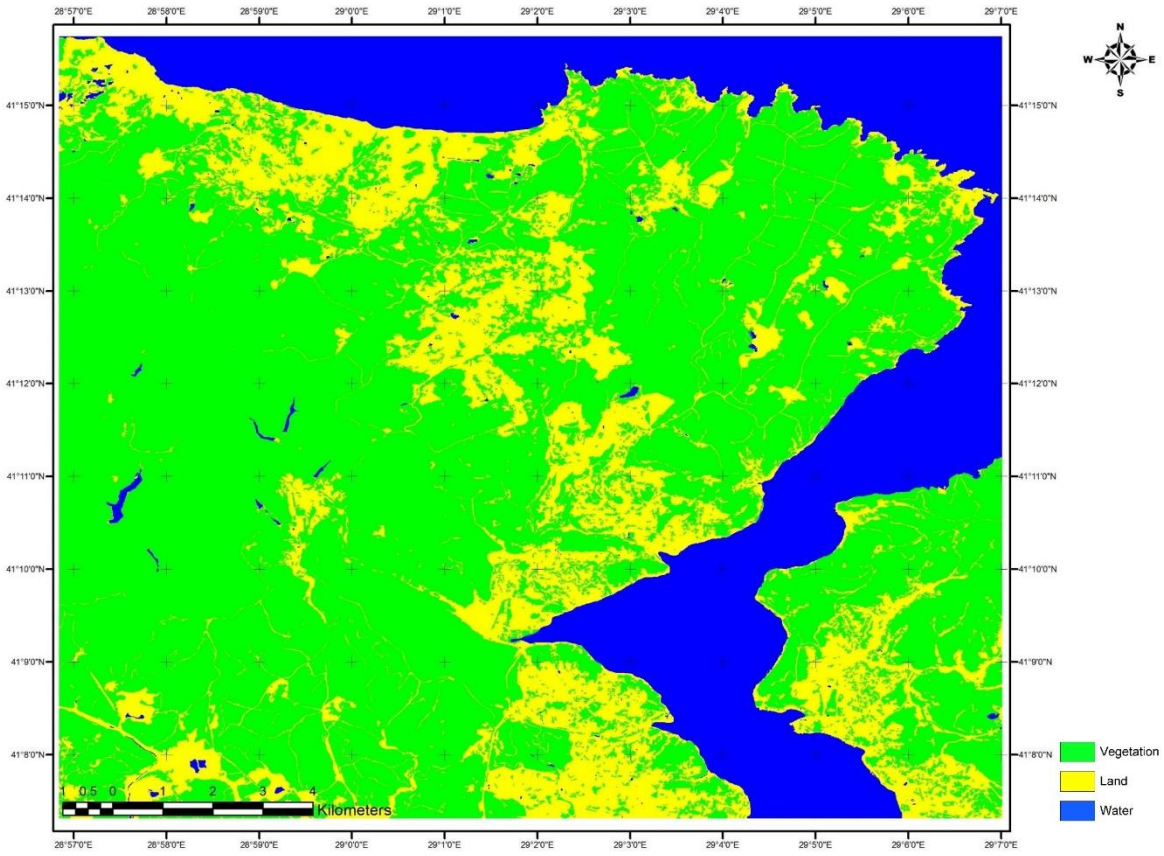


Figure 7. Land, water and vegetation classification results.

In the second step, deciduous, coniferous and shrub classifications were made (Figure 8). In this context, overall classification accuracy and Kappa statistic were obtained as 99.33% and 0.99 respectively.

In the final step, a class has been established for each species with a proportionately greater than 5 percent area in the study area. In this context, Oak sp., anatolian chesnut, oriental beech, common hornbeam, black pine, maritime pine and stone pine stands were classified. However, black pine and maritime pine stands which are spectrally similar and lower the classification accuracy were evaluated in a single class. After the classifications, water bodies and land classes were merged to the obtained thematic data and accuracy assessments were made for 8 classes (Table 4, Figure 9).

As mentioned before, by using the bottom-up approach, the generability of individual tree-based information were examined. In this context, three different scenario or forest stand structure were evaluated. Individual trees were classified and accuracy assessments were performed. The number of trees obtained by stereoscopic interpretation was used as a reference in the accuracy assessment stage.

First plot site was selected in a coniferous (Maritime pine) forest with complete crown closure. Using a multi-stage classification method, top point of each trees and the gaps between trees were determined. In addition, an iterative algorithm was prepared using bottom-up segmentation technique and the crown boundaries were determined (Figure 10). According to accuracy assessment results overall classification accuracy was obtained as 94.74% (Table 5).

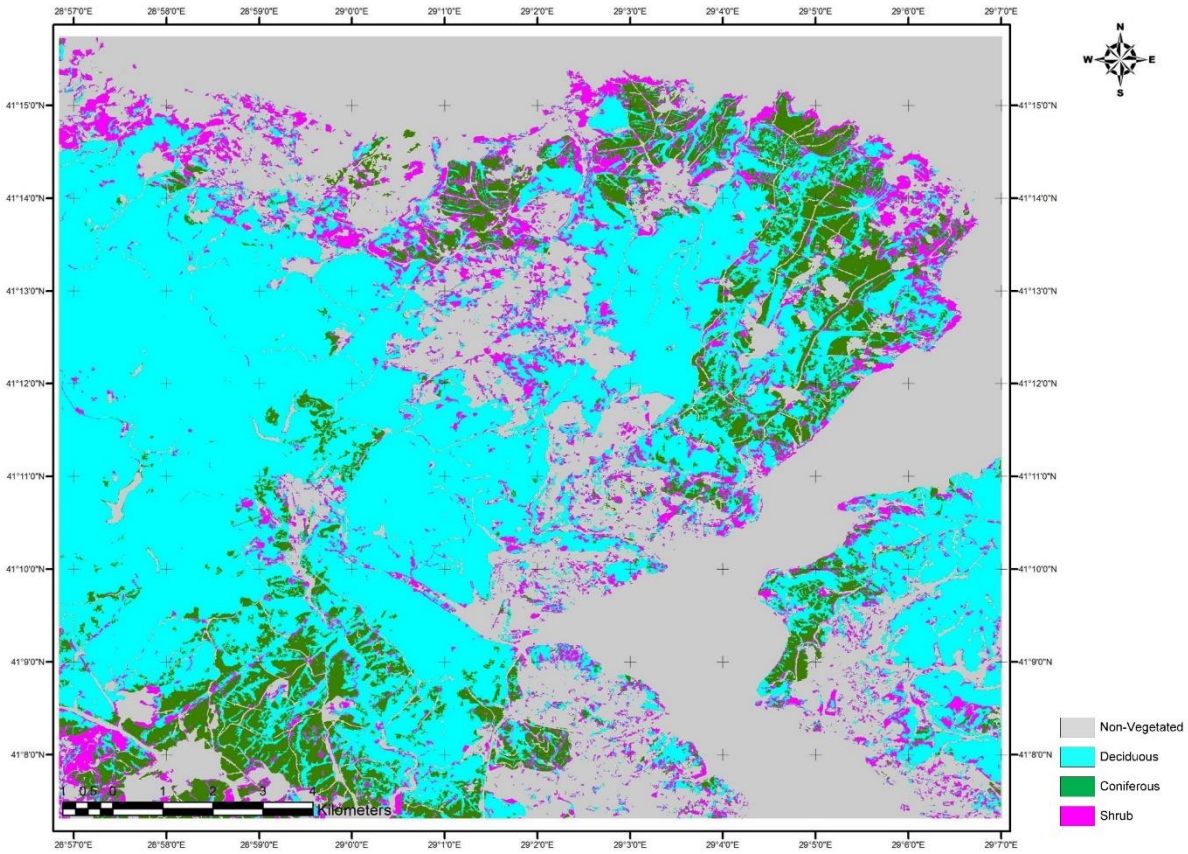


Figure 8. Deciduous, coniferous and shrub classification results.

Table 4. Classification accuracies for all classes.

| Class name | Producer's Accuracy | User's Accuracy | Kappa |
|---|---|---|---|
| Land | 100.00% | 100.00% | 1.0000 |
| Water bodies | 100.00% | 100.00% | 1.0000 |
| Oak sp. | 100.00% | 100.00% | 1.0000 |
| Anatolian chesnut | 89.47% | 94.44% | 0.9360 |
| Oriental beech | 94.44% | 94.44% | 0.9365 |
| Common hornbeam | 88.24% | 83.33% | 0.8110 |
| Black pine - Maritime pine | 94.44% | 94.44% | 0.9365 |
| Stone pine | 94.44% | 94.44% | 0.9365 |
| Overall Classification Accuracy | | 95.14% | |
| Overall Kappa Statistics | | 0.9444 | |

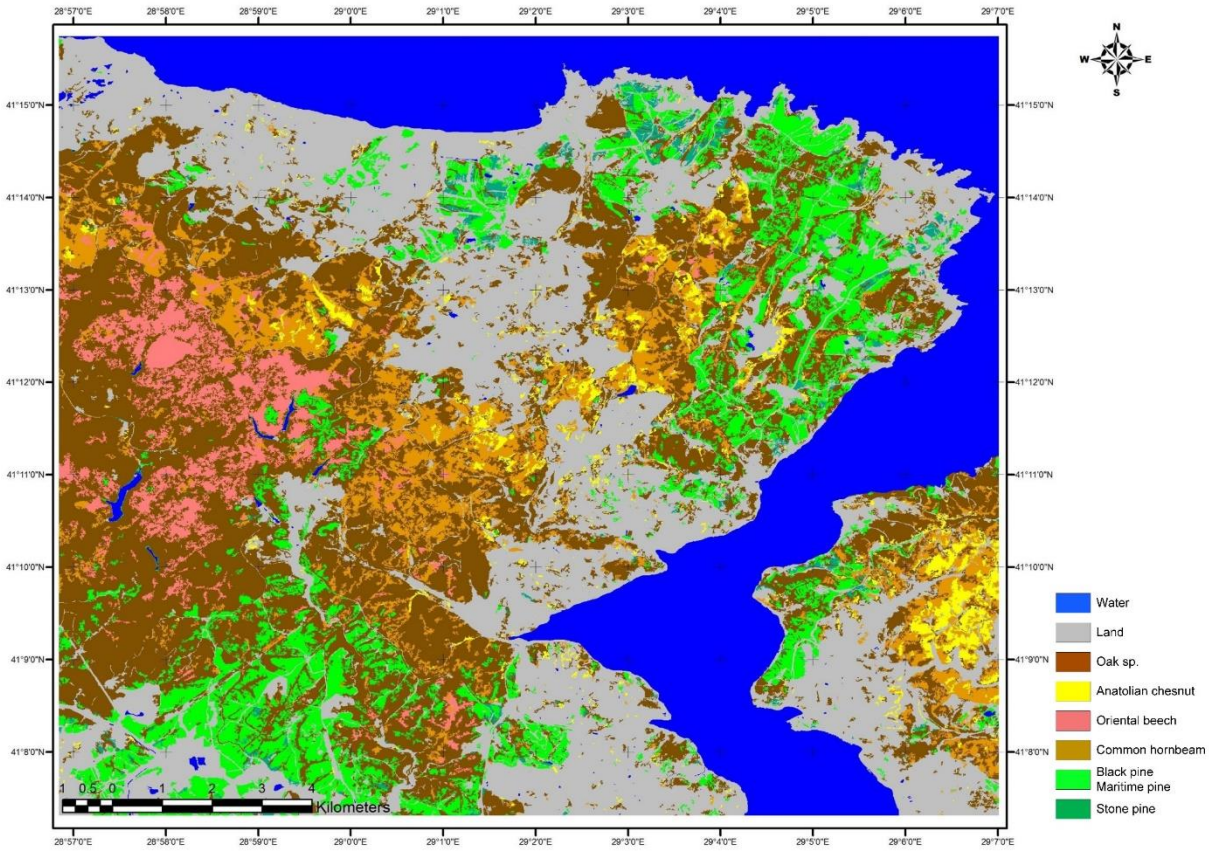


Figure 9. Classification results for all classes.

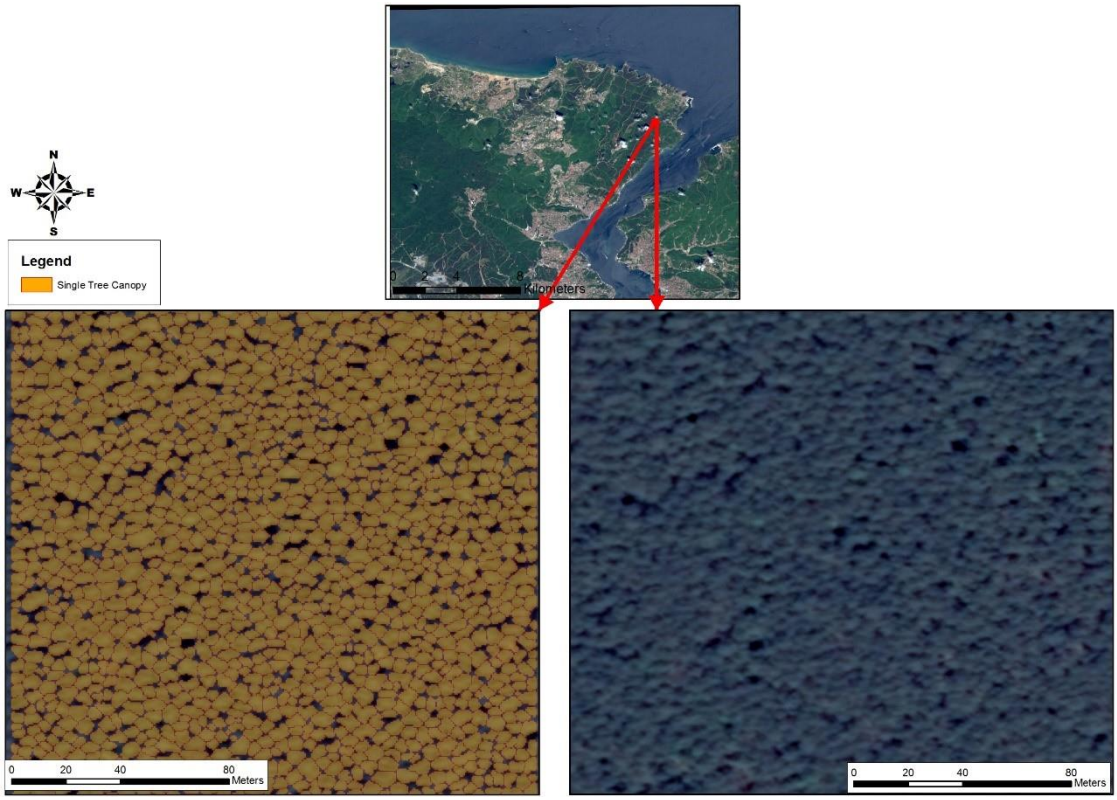


Figure 10. Classification of coniferous (Maritime pine) forest with complete crown closure.

Table 5. Accuracy assessment result of coniferous (Maritime pine) forest with complete crown closure.

| Number of trees obtained by photogrammetric evaluations | Total number of trees as a result of classification | Number of extra trees that do not actually exist | Number of trees that cannot actually be detected | Total Number of Incorrectly Classified Trees |
|---|---|---|---|---|
| 228 | 232 | 10 | 6 | 16 |
| Overall Classification Accuracy | 94,74% | | | |
| Error of Omission | 6,90% | | | |
| Producer's accuracy | 93,10% | | | |

Second plot site was selected in a coniferous (Stone pine) forest with sparse crown closure. Using a multi-stage classification method, bare earth, highway, leafy and coniferous trees were classified separately. Similarly to the first plot site, an iterative algorithm was prepared using bottom-up segmentation technique and the crown boundaries were determined (Figure 11). According to accuracy assessment results overall classification accuracy was obtained as 100% (Table 6).


Figure 11. Classification of coniferous (Stone pine) forest with sparse crown closure

## Conclusions

The main purpose of this study is to investigate what data can be obtained from high resolution satellite data by using object-oriented image analysis methods for forestry purposes. In the context of this study, the most important point encountered during the study and the literature research was the lack of a standard workflow in the object-based image analysis method. Therefore, the user has to decide the

Table 6. Accuracy assessment result of coniferous (Stone pine) forest with sparse crown closure

| Number of trees obtained by photogrammetric evaluations | Total number of trees as a result of classification | Number of extra trees that do not actually exist | Number of trees that cannot actually be detected | Total Number of Incorrectly Classified Trees |
|---|---|---|---|---|
| 264 | 267 | 3 | 0 | 3 |
| Overall Classification Accuracy | 100,00% | | | |
| Error of Omission | 1,12% | | | |
| Producer's accuracy | 98,88% | | | |

appropriate methods according to the data and the desired outputs. The preparation of rule sets with a high classification accuracy depends entirely on the operator's knowledge and experience.

The final plot site was selected in a deciduous (Oak sp., Oriental beech, Common hornbeam) forest with complete crown closure. Despite all the evaluations, it was not possible to obtain individual tree based data for forest areas in this structure (Figure 12). The main reason of this situation was considered as the sympodial branching of deciduous species.

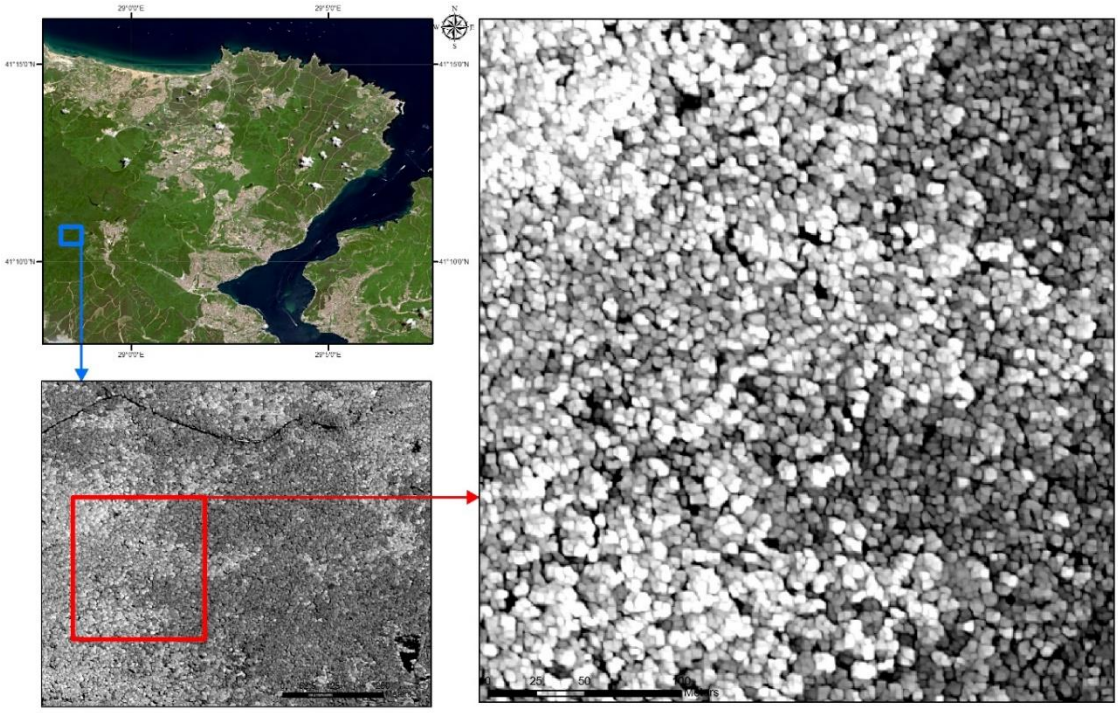

Figure 12. Image objects of deciduous forest with complete crown closure

In the decision-making process, the user needs to know the attributes of the objects he / she is working on, as well as which variables will be defined in a mathematical model. One of the findings obtained from the study is that the rule sets prepared for a specific object or class give much more accurate results than the rule sets prepared for obtaining many objects. In addition, it has been found that the preparation and implementation of such rule sets are more efficient.

In accordance with the results presented in the study, data, which are very important in terms of forestry such as number of trees per hectare and tree crown width, were obtained with satisfactory accuracy by using OBIA and VHR satellite imagery.

**Acknowledgments**

This paper is based in part on a PhD thesis of Huseyin Yurtseven under the supervision of Hakan Yener completed in 2014 at Istanbul University, Science Institute. This work was supported by Scientific Research Projects Coordination Unit of Istanbul University. The project number is 9895.

**References**

Aplin, P., Atkinson, P. M., Curran, P. J. (1999). Fine spatial resolution simulated satellite sensor imagery for land cover mapping in the United Kingdom. Remote Sensing of Environment, 68(3), 206-216.

Baatz, M., Benz, U., Dehghani, S., Heynen, M., Höltje, A., Hofmann, P., Lingenfelder, I., Mimler, M., Sohlbach, M., Weber, M. (2004). eCognition professional user guide 4. Munich: Definiens Imaging.

Baatz, M., Schäpe, A. (1999). Object-oriented and multi-scale image analysis in semantic networks. 2nd international symposium: operationalization of remote sensing, pp. 16-20.

Bakker, W. H., Janssen, L. L. F., Reeves, C. V., Gorte, B. G. H., Christine, P., Weir, M. J. C., Horn, J. A., Anupma, P., Tsehaie, W. (2009). Principles of Remote Sensing: An Introductory Textbook. Enschede, The Netherlands.

Baltsavias, E. P. (2004). Object extraction and revision by image analysis using existing geodata and knowledge: Current status and steps towards operational systems. ISPRS Journal of Photogrammetry and Remote Sensing, 58(3-4), 129-151.

Blaschke, T. (2010). Object based image analysis for remote sensing. ISPRS Journal of Photogrammetry and Remote Sensing, 65(1), 2-16.

Blaschke, T., Hay, G. J., Kelly, M., Lang, S., Hofmann, P., Addink, E., Queiroz Feitosa, R., van der Meer, F., van der Werff, H., van Coillie, F., Tiede, D. (2014). Geographic Object-Based Image Analysis – Towards a new paradigm. ISPRS Journal of Photogrammetry and Remote Sensing, 87(0), 180-191.

Blaschke, T., Lang, S., Hay, G. J. (2008). Object-based image analysis : spatial concepts for knowledge-driven remote sensing applications. New York: Springer.

Brandtberg, T., Walter, F. (1998). Automated delineation of individual tree crowns in high spatial resolution aerial images by multiple-scale analysis. Machine Vision and Applications, 11(2), 64-73.

Câmara, G., Souza, R. C. M., Freitas, U. M., Garrido, J. (1996). Spring: Integrating remote sensing and gis by object-oriented data modelling. Computers and Graphics (Pergamon), 20(3), 395-403.

Campbell, J. B., Wynne, R. H. (2012). Introduction to Remote Sensing, Fifth Edition: Guilford Publications.

Chubey, M. S., Franklin, S. E., Wulder, M. A. (2006). Object-based analysis of Ikonos-2 imagery for extraction of forest inventory parameters. Photogrammetric Engineering and Remote Sensing, 72(4), 383.

Cliche, G., Bonn, F., Teillet, P. (1985). Integration of the SPOT panchromatic channel into its multispectral mode for image sharpness enhancement. Photogrammetric Engineering and Remote Sensing, 51, 311-316.

Culvenor, D. S. (2002). TIDA: an algorithm for the delineation of tree crowns in high spatial resolution remotely sensed imagery. Computers & Geosciences, 28(1), 33-44.

de Béthune, S., Muller, F., Donnay, J.-P. (1998). Fusion of multispectral and panchromatic images by local mean and variance matching filtering techniques. Fusion of Earth Data, 28-30.

Descombes, X., Pechersky, E. (2006). Tree crown extraction using a three states Markov random field. INRIA.

Deskevich, M. P., Padwick, C. (2012). System and Method For Combining Color Information With Spatial Information In Multispectral Images. United States.

Erdin, K. (1986). Fotoyorumlama ve Uzaktan Algılama. İstanbul: İstanbul Üniversitesi Orman Fakültesi Yayınları.

Erikson, M. (2003). Segmentation of individual tree crowns in colour aerial photographs using region growing supported by fuzzy rules. Canadian Journal of Forest Research, 33(8), 1557-1563.

Garguet-Duport, B., Girel, J., Chassery, J.-M., Patou, G. (1996). The use of multiresolution analysis and wavelets transform for merging SPOT panchromatic and multispectral image data. Photogrammetric Engineering and Remote Sensing, 62(9), 1057-1066.

Gougeon, F. A. (1995). A crown-following approach to the automatic delineation of individual tree crowns in high spatial resolution aerial images. Canadian Journal of Remote Sensing, 21(3), 274–284.

Gudex-Cross, D., Pontius, J., Adams, A. (2017). Enhanced forest cover mapping using spectral unmixing and object-based classification of multi-temporal Landsat imagery. Remote Sensing of Environment, 196, 193-204.

Haralick, R. M. (1983). Decision Making In Context. IEEE Transactions on Pattern Analysis and Machine Intelligence, PAMI-5(4), 417-428.

Haralick, R. M., Shapiro, L. G. (1985). Image Segmentation Techniques. Computer Vision, Graphics, and Image Processing, 29(1), 100-132.

Hay, G., Niemann, K., McLean, G. (1996). An object-specific image-texture analysis of H-resolution forest imagery. Remote Sensing of Environment, 55(2), 108-122.

Hayes, D. J., Sader, S. A., Schwartz, N. B. (2002). Analyzing a forest conversion history database to explore the spatial and temporal characteristics of land cover change in Guatemala's Maya Biosphere Reserve. Landscape Ecology, 17(4), 299-314.

Henrich, V., Krauss, G., Götze, C., Sandow, C. (2015). IDB - Index Database: A database for remote sensing indices.

Huete, A., Liu, H., Batchily, K., Van Leeuwen, W. (1997). A comparison of vegetation indices over a global set of TM images for EOS-MODIS. Remote Sensing of Environment, 59(3), 440-451.

Immitzer, M., Vuolo, F., Atzberger, C. (2016). First Experience with Sentinel-2 Data for Crop and Tree Species Classifications in Central Europe. Remote Sensing, 8(3).

Jackson, R., Slater, P., Pinter Jr, P. (1983). Discrimination of growth and water stress in wheat by various vegetation indices through clear and turbid atmospheres. Remote Sensing of Environment, 13(3), 187-208.

Jones, D., Pike, S., Thomas, M., Murphy, D. (2011). Object-based image analysis for detection of Japanese knotweed sl taxa (Polygonaceae) in Wales (UK). Remote Sensing, 3(2), 319-342.

Kaczynski, R., Donnay, J.-P., Muller, F. (1995). Satellite image maps of Warsaw in the scale 1: 25,000. EARSeL Advances in Remote Sensing, 4, 100-102.

Kaufman, Y. J., Tanré, D. (1996). Strategy for direct and indirect methods for correcting the aerosol effect on remote sensing: from AVHRR to EOS-MODIS. Remote Sensing of Environment, 55(1), 65-79.

Ke, Y., Quackenbush, L. J. (2007). Forest species classification and tree crown delineation using Quickbird imagery. Proceedings of the ASPRS 2007 Annual Conference, pp. 7-11.

Kettig, R. L., Landgrebe, D. (1976). Classification of multispectral image data by extraction and classification of homogeneous objects. Geoscience Electronics, IEEE Transactions on, 14(1), 19-26.

Koç, A. (1997). Belgrad Ormanındaki Ağaç Türü Ve Karışımlarının Uydu Verileri Ve Görüntü İşleme Teknikleri İle Belirlenmesi. İ.Ü. Orman Fakültesi Dergisi, A/47(1), 89-110.

Levine, M. D., Nazif, A. M. (1985). Rule-based image segmentation: a dynamic control strategy approach. Computer Vision, Graphics, & Image Processing, 32(1), 104-126.

Li, D., Ke, Y., Gong, H., Li, X. (2015). Object-Based Urban Tree Species Classification Using Bi-Temporal WorldView-2 and WorldView-3 Images. Remote Sensing, 7(12).

Lillesand, T., Kiefer, R. W., Chipman, J. (2014). Remote Sensing and Image Interpretation: Wiley.

Lobo, A. (1997). Image segmentation and discriminant analysis for the identification of land cover units in ecology. Geoscience and Remote Sensing, IEEE Transactions on, 35(5), 1136-1145.

Lobo, A., Chic, O., Casterad, A. (1996). Classification of Mediterranean crops with multisensor data: Per-pixel versus per-object statistics and image segmentation. International Journal of Remote Sensing, 17(12), 2385-2400.

McKeown Jr, D. M., Harvey, W. A., Wixson, L. E. (1989). Automating knowledge acquisition for aerial image interpretation. Computer Vision, Graphics, & Image Processing, 46(1), 37-81.

Navulur, K. (2007). Multispectral Image Analysis Using the Object-Oriented Paradigm: CRC Press/Taylor & Francis.

Neubert, M., Meinel, G. (2005). Atmospheric and terrain correction of Ikonos imagery using ATCOR3. Leibniz Institute of Ecological and Regional Development. Dresden, Germany.

Nussbaum, S. (2008). Object-based image analysis and treaty verification : new approaches in remote sensing - applied to nuclear facilities in iran. New York, NY: Springer Berlin Heidelberg.

Padwick, C., Deskevich, M., Pacifici, F., Smallwood, S. (2010). WorldView-2 pan-sharpening. Proc. American Society for Photogrammetry and Remote Sensing, 13.

Pal, N. R., Pal, S. K. (1993). A review on image segmentation techniques. Pattern Recognition, 26(9), 1277-1294.

Perrin, G., Descombes, X., Zerubia, J. (2006). A non-Bayesian model for tree crown extraction using marked point processes. INRIA.

Pinz, A. (1989). Final results of the vision expert system VES: finding trees in aerial photographs. Wissensbasierte Mustererkennung. Wien, 49, 90-111.

Pollock, R. J. (1996). The automatic recognition of individual trees in aerial images of forests based on a synthetic tree crown image model. The University of British Columbia (Canada).

Rafieyan, O., Darvishsefat, A., Babaii, S. (2009a). Evaluation of object-based classification method in forest applications using UltraCamD imagery (Case study: Northern forest of Iran). 3rd National Forest Congress. University of Tehran, Karaj, Iran.

Rafieyan, O., Darvishsefat, A., Babaii, S., Mataji, A. (2009b). Object-based classification using UltraCam-D images for tree species discrimination (Case study: Hyrcanian Forest-Iran). The International Archives of the Photogrammetry, Remote Sensing and Spatial Information Sciences, 38.

Richter, R., Schläpfer, D. (2014). Atmospheric/Topographic Correction For Satellite Imagery. Switzerland: ReSe Applications Schlapfer.

Rouse Jr, J., Haas, R., Schell, J., Deering, D. (1974). Monitoring vegetation systems in the Great Plains with ERTS. NASA special publication, 351, 309.

Ryherd, S., Woodcock, C. (1996). Combining spectral and texture data in the segmentation of remotely sensed images. Photogrammetric Engineering and Remote Sensing, 62(2), 181-194.

Sader, S., Winne, J. (1992). RGB-NDVI colour composites for visualizing forest change dynamics. International Journal of Remote Sensing, 13(16), 3055-3067.

Sandmann, H., Lertzman, K. P. (2003). Combining high-resolution aerial photography with gradient-directed transects to guide field sampling and forest mapping in mountainous terrain. Forest Science, 49(3), 429-443.

Schott, J. R. (2007). Remote sensing : the image chain approach. New York: Oxford University Press.

Sellers, P. (1985). Canopy reflectance, photosynthesis and transpiration. International Journal of Remote Sensing, 6(8), 1335-1372.

Strahler, A. H., Woodcock, C. E., Smith, J. A. (1986). On the nature of models in remote sensing. Remote Sensing of Environment, 20(2), 121-139.

Trimble (2012). eCognition Developer User Guide. München: Trimble Germany GmbH.

Tucker, C. J. (1979). Red and photographic infrared linear combinations for monitoring vegetation. Remote Sensing of Environment, 8(2), 127-150.

Updike, T., Comp, C. (2010). Radiometric use of WorldView-2 imagery. Technical Note, 1-17.

Welch, R., Ehlers, M. (1987). Merging multiresolution SPOT HRV and Landsat TM data. Photogrammetric Engineering and Remote Sensing, 53, 301-303.

Wolf, A. (2010). Using WorldView 2 Vis-NIR MSI imagery to support land mapping and feature extraction using normalized difference index ratios. DigitalGlobe 8-Band Research Challenge, 1-13.

Wong, T., Mansor, S., Mispan, M., Ahmad, N., Sulaiman, W. (2003). Feature extraction based on object oriented analysis. Proceedings of ATC 2003 Conference, pp. 20-21.

Wu, B., Yu, B., Wu, Q., Huang, Y., Chen, Z., Wu, J. (2016). Individual tree crown delineation using localized contour tree method and airborne LiDAR data in coniferous forests. International Journal of Applied Earth Observation and Geoinformation, 52, 82-94.

Wulder, M. (1998). Optical remote-sensing techniques for the assessment of forest inventory and biophysical parameters. Progress in Physical Geography, 22(4), 449-476.

Wulder, M. A., White, J. C., Hay, G. J., Castilla, G. (2008). Towards automated segmentation of forest inventory polygons on high spatial resolution satellite imagery. The Forestry Chronicle, 84(2), 221-230.

Yan, G., Mas, J. F., Maathuis, B., Xiangmin, Z., Van Dijk, P. (2006). Comparison of pixel-based and object-oriented image classification approaches—a case study in a coal fire area, Wuda, Inner Mongolia, China. International Journal of Remote Sensing, 27(18), 4039-4055.

Yu, Q., Gong, P., Clinton, N., Biging, G., Kelly, M., Schirokauer, D. (2006). Object-based detailed vegetation classification with airborne high spatial resolution remote sensing imagery. Photogrammetric Engineering and Remote Sensing, 72(7), 799-811.

Yurtseven, H. (2014). Yüksek Çözünürlüklü Uydu Verileri ile Obje Tabanlı Görüntü Analizleri. Fen Bilimleri Enstitüsü. İstanbul, Türkiye: İstanbul Üniversitesi, p. 147.

Zhou, X., Jancsó, T., Chen, C., Verőné, M. W. (2012). Urban Land Cover Mapping Based on Object Oriented Classification Using WorldView 2 Satellite Remote Sensing Images. International Scientific Conference on Sustainable Development & Ecological Footprint. Sopron, Hungary.

Submitted: 07.08.2019 Accepted: 20.08.2019